



HAL
open science

Hydraulic conductivity field characterization from the joint inversion of hydraulic heads and self-potential data

A Soueid Ahmed, Abderrahim Jardani, A Revil, Jean-Paul Dupont

► To cite this version:

A Soueid Ahmed, Abderrahim Jardani, A Revil, Jean-Paul Dupont. Hydraulic conductivity field characterization from the joint inversion of hydraulic heads and self-potential data. *Water Resources Research*, 2014, 50 (4), pp.3502–3522. 10.1002/2013wr014645 . hal-01742277

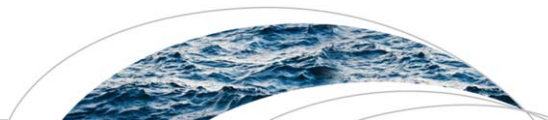
HAL Id: hal-01742277

<https://normandie-univ.hal.science/hal-01742277>

Submitted on 20 May 2021

HAL is a multi-disciplinary open access archive for the deposit and dissemination of scientific research documents, whether they are published or not. The documents may come from teaching and research institutions in France or abroad, or from public or private research centers.

L'archive ouverte pluridisciplinaire **HAL**, est destinée au dépôt et à la diffusion de documents scientifiques de niveau recherche, publiés ou non, émanant des établissements d'enseignement et de recherche français ou étrangers, des laboratoires publics ou privés.



RESEARCH ARTICLE

10.1002/2013WR014645

Hydraulic conductivity field characterization from the joint inversion of hydraulic heads and self-potential data

A. Soueid Ahmed¹, A. Jardani¹, A. Revil^{2,3}, and J. P. Dupont¹

Key Points:

- Self-potential and head data are complementary to assess permeability
- A joint inversion is proposed using the adjoint-state approach
- Five synthetic case studies are evaluated

Correspondence to:

A. Revil,
arevil@mines.edu

Citation:

Soueid Ahmed, A., A. Jardani, A. Revil, and J. P. Dupont (2014), Hydraulic conductivity field characterization from the joint inversion of hydraulic heads and self-potential data, *Water Resour. Res.*, 50, 3502–3522, doi:10.1002/2013WR014645.

Received 24 AUG 2013

Accepted 9 APR 2014

Accepted article online 15 APR 2014

Published online 29 APR 2014

¹CNRS, UMR 6143, M2C, Morphodynamique Continentale et Côtière, Université de Rouen, Mont-Saint-Aignan, France,

²Department of Geophysics, Colorado School of Mines, Golden, Colorado, USA, ³ISTerre, CNRS, UMR 5275, Equipe Volcan, Université de Savoie, Le Bourget-du-Lac, France

Abstract Pumping tests can be used to estimate the hydraulic conductivity field from the inversion of hydraulic head data taken intrusively in a set of piezometers. Nevertheless, the inverse problem is strongly underdetermined. We propose to add more information by adding self-potential data taken at the ground surface during pumping tests. These self-potential data correspond to perturbations of the electrical field caused directly by the flow of the groundwater. The coupling is electrokinetic in nature that is due to the drag of the excess of electrical charges existing in the pore water. These self-potential signals can be easily measured in field conditions with a set of the nonpolarizing electrodes installed at the ground surface. We used the adjoint-state method for the estimation of the hydraulic conductivity field from measurements of both hydraulic heads and self potential during pumping tests. In addition, we use a recently developed petrophysical formulation of the streaming potential problem using an effective charge density of the pore water derived directly from the hydraulic conductivity. The geostatistical inverse framework is applied to five synthetic case studies with different number of wells and electrodes and thickness of the confining unit. To evaluate the benefits of incorporating the self-potential data in the inverse problem, we compare the cases in which the data are combined or not. Incorporating the self-potential information improves the estimate of hydraulic conductivity field in the case where the number of piezometers is limited. However, the uncertainty of the characterization of the hydraulic conductivity from the inversion of the self-potential data is dependent on the quality of the distribution of the electrical conductivity used to solve the Poisson equation. Consequently, the approach discussed in this paper requires a precise estimate of the electrical conductivity distribution of the subsurface and requires therefore new strategies to be developed for the joint inversion of the hydraulic and electrical conductivity distributions.

1. Introduction

The characterization of hydraulic conductivity (K -) field (in m s^{-1}) of an aquifer constitutes a crucial aspect in the modeling of groundwater flow, the transport of contaminants, and their remediation. The hydraulic conductivity is usually determined from hydrogeological (invasive) methods such as pumping tests and requiring a set of piezometers [Bear, 1988].

In hydrogeology, various techniques have been proposed for mapping the hydraulic conductivity field from a sequence of pumping tests. Yeh *et al.* [1996] and Zhang and Yeh [1997] have developed an iterative geostatistical inverse method in which a successive linear estimator (SLE) was used to include the nonlinear relationship between the hydraulic parameters and the hydraulic heads. Such type of technique was validated both in the laboratory, using sandbox experiments [Liu *et al.*, 2002, 2007], and in field conditions [Straface *et al.*, 2007; Cardiff *et al.*, 2009]. Kuhlman *et al.* [2008] applied the SLE approach at the scale of a catchment while Cardiff *et al.* [2009] used recently the quasi-linear statistical approach of Kitanidis [1996] to image the distribution of the hydraulic conductivity at the Boise Hydrogeophysical Research Site (BHRS). Recent developments in the field of hydraulic tomography include the works by Hernandez *et al.* [2006], Liu *et al.* [2007], Straface *et al.* [2007], Cardiff *et al.* [2009], Brauchler *et al.* [2013], Mao *et al.* [2013], and references therein.

The inverse problem in hydraulic tomography is strongly nonunique and underdetermined. The resolution of the hydraulic conductivity field depends strongly on the density of piezometers. In general, a limited number of available piezometers imply a poor reconstruction of the hydraulic conductivity field of

heterogeneous aquifers, which can be an issue for some hydrogeological problems. To reduce this issue, researchers have been looking at possible sources of additional information to help constrain the inverse problem or using various regularizers to shape the objective function to minimize the nonuniqueness of the solution and to provide solutions with given additional characteristics.

Various geophysical methods can be used to provide additional information to the hydraulic tomography problem. Electrical resistivity tomography (ERT) has been broadly used, alone, or in combination with other data sources, to estimate the hydraulic conductivity field [see, for instance, *Troisi et al.*, 2000; *Bowling et al.*, 2006; *Bohling and Butler*, 2010; *Pollock and Cirpka*, 2010]. Another relevant method is induced polarization, which is an extension of ERT to include low-frequency (0.1–100 Hz in field conditions) polarization effects. In this case, the electrical conductivity is replaced by a complex conductivity with in-phase and quadrature components. The complex conductivity can be used, in turn, to determine or to image the hydraulic conductivity field (see *Hördt et al.* [2006] for a field application and *Revil and Florsch* [2010], *Revil et al.* [2012], and *Revil* [2013] for the development of new petrophysical models). Two other popular geophysical approaches in hydrogeophysics have been the use of the ground-penetrating radar (GPR) and seismic surveys [e.g., *Hyndman et al.*, 2000; *Chen et al.*, 2001].

In this paper, we follow the old idea proposed in hydrogeology by *Abaza and Clyde* [1969] to use the self-potential data in getting information on flow rate and the hydraulic conductivity field. A description of the early history of the use of the self-potential method to characterize groundwater flow can be found in *Revil et al.* [2012] and *Revil and Jardani* [2013] and will not be repeated here. The self-potential signals correspond to the passive measurements of the electric potential field (or its fluctuations) recorded at the ground surface of the Earth or in boreholes with a set of nonpolarizable electrodes [e.g., *Petiau and Dupis*, 1980; *Petiau*, 2000], and using a high-impedance voltmeter (typically >10 M Ω). The first hydrogeophysical observation that groundwater flow produces a recordable electrical field was made by the Russian-born Physicist Porphyry Ivanovich Bachmetjew [*Bachmetjew*, 1896]. The physics of this “streaming potential” was developed earlier by *Quincke* [1859], first conceptualized by *Helmholtz* [1879], and later by *von Smoluchowski* [1903]. *Bogoslovsky and Ogilvy* [1973] and *Semenov* [1980] were probably the first to apply the self-potential method to pumping tests. *Jardani and Revil* [2009] used self-potential and temperature data in a geothermal field to invert the piecewise constant hydraulic conductivity distribution using a stochastic method and known facies boundaries. In the present paper, we are looking for the reconstruction of the hydraulic conductivity field from the joint inversion of the hydraulic head and self-potential data associated with pumping tests.

The self-potential signals are generated by the drag of the excess of electrical charges contained in the pore water, more precisely in the electrical diffuse layer coating the surface of the minerals [*Kulesa et al.*, 2003; *Revil et al.*, 2003; *Jardani et al.*, 2006]. The electrical double layer is formed of (1) the Stern layer [*Stern*, 1924] that is attached to the mineral surface and (2) the diffuse layer [*Gouy*, 1910; *Chapman*, 1913] that is mobile and can be partly dragged by the flow of the pore water. The resulting electrical current density (flux of electrical charges per unit surface area per unit time) is known as the streaming current density and the associated electrical field is often called (improperly) the streaming potential [*Bogoslovsky and Ogilvy*, 1973]. A general theory of the streaming current in poroelastic and unsaturated porous rocks and soils can be found in *Revil and Mahardika* [2013]. Due to its sensitivity to the water motion in the porous medium, the self-potential method has been used to monitor hydraulic head changes associated with pumping tests [for instance, *Semenov*, 1980; *Rizzo et al.*, 2004; *Titov et al.*, 2005; *Maineult et al.*, 2008; *Jardani et al.*, 2009; *Straface et al.*, 2010, 2011]. These works have been mostly focused on showing the existence of recordable signals, in performing forward modeling of the self-potential response, and in developing simple interpretation schemes, mostly based on the linear relationship between the changes in the self-potential signals and the concomitant changes in hydraulic heads. We will avoid these types of relationships (for instance, directly between the head the self-potential signals) in our analysis. *Malama et al.* [2009a, 2009b] developed recently the mathematical solutions for the self-potential responses associated with pumping tests in both confined and unconfined homogeneous aquifers. Their semianalytical solutions can be very useful in benchmarking numerical codes but they do not account for the heterogeneous character of aquifers. This approach has been extended recently by *Malama* [2014] to account for the flow in the vadose zone during pumping tests in an unconfined aquifer.

We need also to consider the petrophysical model for the streaming potential coupling coefficient, a key sensitivity parameter entering into the determination of the self-potential signals. *Jardani et al.* [2007]

introduced an empirical relationship to compute self-potential signals of electrokinetic nature using an effective volumetric charge density. This parameter can be inferred directly from the hydraulic conductivity, which reduces the number of petrophysical parameters needed to invert the hydraulic conductivity from self-potential data. The validity and uncertainty associated with this relationship will be discussed below.

We are interested in developing a novel formulation to infer directly from the joint inversion of self-potential and head data the hydraulic conductivity field of a heterogeneous aquifer in 3-D. Our approach is based on the adjoint-state method to compute the sensitivity matrix of the self-potential observations to the hydraulic conductivity. Our goal is to underline the strengths and weaknesses of the self-potential method for determining K -fields during pumping tests.

2. Forward Problem

In this section, we define the fundamental equations used to simulate the streaming potential signals in the quasi-static regime of the Maxwell equations and for steady state groundwater flow conditions for a confined aquifer. The forward problem of the self potential requires the coupling of both the hydraulic and electric problems. That said, the electro-osmotic contribution in the Darcy velocity is negligible and the problem can be partially decoupled (the electrical field is generated by the flow of the pore water but does not measurably influence the Darcy velocity itself, [e.g., *Revil et al.*, 1999]).

For an isotropic, heterogeneous, and water-saturated porous material, the hydraulic problem can be expressed for an aquifer in steady state conditions using the following continuity and constitutive equations,

$$\nabla \cdot \mathbf{u} = Q_s, \tag{1}$$

$$\mathbf{u} = -K\nabla h, \tag{2}$$

respectively, where \mathbf{u} denotes the Darcy velocity (in m s^{-1}), h denotes the hydraulic head (in m), K (in m s^{-1}) is the saturated hydraulic conductivity (a scalar for isotropic formations), and Q_s (in s^{-1}) represents the external hydraulic sources/sinks due to the pumping/injection tests. Equations (1) and (2) are subjected to the following boundary conditions for the synthetic tests developed below (other boundary conditions may exist for other problems):

$$h = h_D \text{ at } \Gamma_D, \tag{3}$$

$$-\mathbf{n} \cdot K\nabla h = 0 \text{ at } \Gamma_N. \tag{4}$$

In these equations, the constant hydraulic head h_D is imposed at the boundary Γ_D , \mathbf{n} is the unit vector normal to the boundary Γ_N . Equations (3) and (4) correspond to the Dirichlet and Neumann boundary conditions, respectively. We will discuss further the boundary conditions for our synthetic case study in section 4.

We first present the boundary-value problem for the self-potential field. In an isotropic heterogeneous media, the total current density \mathbf{j} (in A m^{-2} ; representing the total flux of electrical charges) is the sum of a conductive current density (given by Ohm's law) plus a source current density called the streaming current [e.g., *Jardani et al.*, 2007]:

$$\mathbf{j} = -\sigma\nabla\varphi + \hat{Q}_V\mathbf{u}, \tag{5}$$

where φ is the electrical (self-)potential (in V), σ is the electrical conductivity of the porous material (in S m^{-1} ; a scalar in isotropic conditions), and \hat{Q}_V (in C m^{-3}) is the effective excess charge density per unit pore volume that is dragged by the flow of the pore water. This charge density represents a fraction of the total charge density of the electrical diffuse layer. The charge density \hat{Q}_V can be directly predicted from the hydraulic conductivity K (m s^{-1}) according to the empirical relationships established by *Jardani et al.* [2007]:

$$\log_{10}\hat{Q}_V = -3.49 - 0.82\log_{10}K, \tag{6}$$

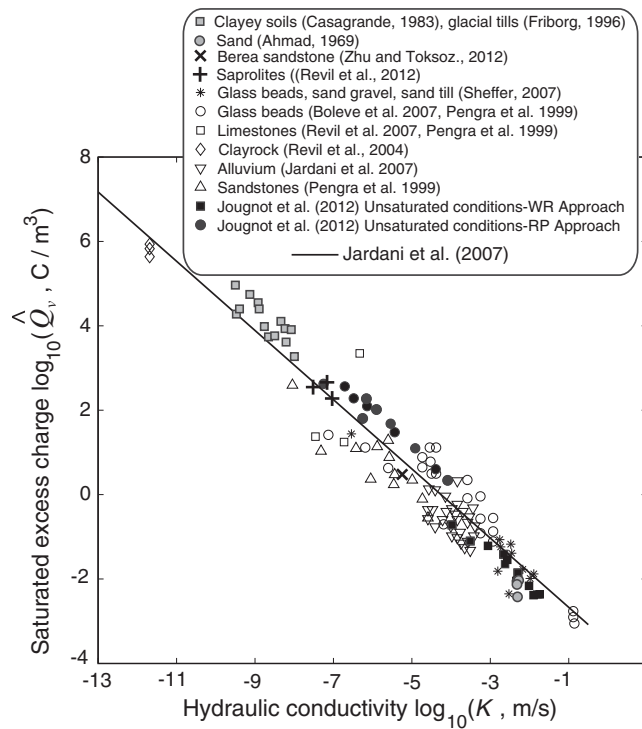


Figure 1. Quasi-static charge density \hat{Q}_v (excess pore charge moveable by the quasi-static pore water flow) versus the hydraulic conductivity K for a broad collection of core samples and porous materials. Data from Ahmad [1969], Bolève et al. [2007], Casagrande [1983], Friborg [1996], Jougnot et al. [2012], Jardani et al. [2007], Pengra et al. [1999], Revil et al. [2004, 2007], Sheffer [2007], Revil et al. [2013], and Zhu and Toksöz [2012]. These measurements were performed at various salinities and pH values (pH between 5 and 7 except for the limestones).

The validity of this equation is shown in Figure 1 for a broad variety of rocks and sediments [Jardani et al., 2007]. As shown in Figure 1, there is some uncertainty in predicting the effective charge density with equation (6). This uncertainty is not considered in the present work because the uncertainty in Figure 1 is coming essentially from the fact that the data are not corrected for the effect of salinity (or TDS, total dissolved solid) and pH. For a known pH and mineralization of the pore water, it is likely that the uncertainty in the relationship between the charge density and the permeability will be reduced.

The continuity equation for the electrical charge is $\nabla \cdot \mathbf{j} = 0$ [Sill, 1983], which combined with equation (5) yields the following elliptic equation,

$$\nabla \cdot (\sigma \nabla \varphi) = \nabla \cdot \mathbf{j}_s \quad (7)$$

In equation (7), the source current density \mathbf{j}_s (corresponding to the last term of equation (5)) is given by:

$$\mathbf{j}_s = \hat{Q}_v \mathbf{u}, \quad (8)$$

with the following boundary conditions:

$$\varphi = 0 \text{ at } \Gamma_d, \quad (9)$$

$$-\mathbf{n} \cdot [\sigma \nabla \varphi - \mathbf{j}_s] = 0 \text{ at } \Gamma_N. \quad (10)$$

The Neumann boundary condition Γ_N is imposed at the insulating air-ground interface and a Dirichlet boundary condition Γ_d is imposed at the other boundaries. Equation (8) expressed the idea of proportionality between the streaming current density and the flow rate, an idea that was early explored experimentally by Abaza and Clyde [1969].

Note that our approach can be used to define the streaming potential coupling coefficient as well: $C_I = (\partial \varphi / \partial h)_{\mathbf{j}=0} = -K \hat{Q}_v / \sigma$. This coupling coefficient defines the sensitivity of the electrical potential to a change of hydraulic head under the conditions that the total current density is zero. However, just using a relationship between the head and the potential changes [e.g., Straface et al., 2010, 2011] is not a rigorous approach since it is not based on solving the field equation for the electrical potential obtained by combining the constitutive and continuity equations described above.

In our formulation, the number of the petrophysical parameters is limited to the electrical conductivity and the hydraulic conductivity. In field conditions, an estimate of the electrical conductivity distribution can be derived from electrical resistivity tomography (ERT) or from electromagnetic methods. To avoid having to deal with the joint inversion of resistivity, head, and self-potential data all together, the electrical conductivity distribution is assumed to be known here for three of the case studies presented below. In the fourth

case study, we will focus on the impact of the resistivity distribution on the inversion of the hydraulic conductivity data. Our paper focuses on the characterization of the hydraulic conductivity using head and self-potential data alone with or without the knowledge of the resistivity distribution.

3. Inverse Problem

The inverse problem consists in retrieving the hydraulic conductivity field by fitting jointly or not the hydraulic heads measured in the observations wells and the electric (self-)potential data recorded on the ground surface during a set of pumping tests. To reach this goal, we can minimize an objective function. Such an optimization is severely ill posed as the number of unknown parameters is (usually) far greater than the number of available measurements.

In a Bayesian geostatistical framework, the inverse problem consists to minimize the following objective function [Kitanidis, 1996]:

$$L = \frac{1}{2} \left[\mathbf{d}_{h,\varphi}^{obs} - \Psi(\mathbf{s}) \right]^T \mathbf{V}_{h,\varphi}^{-1} \left[\mathbf{d}_{h,\varphi}^{obs} - \Psi(\mathbf{s}) \right] + \frac{1}{2} (\mathbf{s} - \mathbf{X}\beta)^T \mathbf{Q}^{-1} (\mathbf{s} - \mathbf{X}\beta), \tag{11}$$

where $\mathbf{d}_{h,\varphi}^{obs} = [\mathbf{d}_h^{obs}, \mathbf{d}_\varphi^{obs}]$ ($n \times 1$) denotes the vector of observed data. This vector contains the hydraulic heads (data vector \mathbf{d}_h^{obs}) and the self-potentials data (data vector \mathbf{d}_φ^{obs}). The vector \mathbf{s} ($m \times 1$) is a vector of discrete values of the logarithm of the hydraulic conductivity $\log_{10}K$. The ($n \times n$) diagonal covariance matrix of the measurements errors $\mathbf{V}_{h,\varphi}$ is given by:

$$\mathbf{V}_{h,\varphi} = \begin{bmatrix} \sigma_h^2 \mathbf{I}_{N_h \times N_h} & \mathbf{0} \\ \mathbf{0} & \sigma_\varphi^2 \mathbf{I}_{N_\varphi \times N_\varphi} \end{bmatrix}, \tag{12}$$

where σ_h^2 and σ_φ^2 denote the known variances of the measurement errors of the hydraulic head and self-potential data, respectively, $\mathbf{I}_{N \times N}$ represents the identity matrix of size N , N_h , and N_φ denote the number of the measurements of the hydraulic heads and the streaming potentials, respectively. The vector $\mathbf{E}(\mathbf{s}) = \mathbf{X}\beta$ (implying stationarity of the log K -field) denotes the expected value, \mathbf{X} is a m -vector with 1 for all its elements, β is the (unknown) scalar constant denoting the mean of the parameter field. The matrix \mathbf{Q} ($m \times m$), in equation (11), denotes the spatial covariance matrix of the parameters. In our case, this matrix is derived from a Gaussian variogram but other types of variograms could be used as well. We assume that the structural parameters such as the variances and correlation lengths of the Gaussian variogram are considered known from prior information (e.g., downhole measurements or a geological expertise of the sedimentary/soil structure). However, these geostatistical parameters could be estimated as well using a restricted maximum likelihood approach as demonstrated by Cardiff *et al.* [2012]. The vector $\Psi(\mathbf{s})$ ($n \times 1$) corresponds to the forward problem operator in which the hydraulic heads and the streaming potential data are numerically predicted given a log hydraulic conductivity field \mathbf{s} .

The quasi-linear geostatistical method is based on an iterative process with successive first-order Taylor derivatives evaluated at the last $\tilde{\mathbf{s}}_k$:

$$\Psi(\mathbf{s}) = \Psi(\tilde{\mathbf{s}}_k) + \tilde{\mathbf{H}}_k (\mathbf{s} - \tilde{\mathbf{s}}_k), \tag{13}$$

$$\tilde{\mathbf{H}}_k = \left. \frac{\partial \Psi(\mathbf{s})}{\partial \mathbf{s}} \right|_{\mathbf{s} = \tilde{\mathbf{s}}_k}, \tag{14}$$

and where k denotes the number of the iteration step and $\tilde{\mathbf{H}}_k$ ($m \times n$) is the sensitivity or Jacobian matrix of the measurements with respect to the logarithm of hydraulic conductivity at the estimate $\tilde{\mathbf{s}}_k$. In our case, we point out that the Jacobian matrix is composed of two sensitivity matrices corresponding to the both type of measurements,

$$\tilde{\mathbf{H}}_k = \begin{bmatrix} \tilde{\mathbf{H}}_k^h \\ \tilde{\mathbf{H}}_k^\varphi \end{bmatrix}, \tag{15}$$

where $\tilde{\mathbf{H}}_k^h$ and $\tilde{\mathbf{H}}_k^\varphi$ denote the sensitivity of the hydraulic heads and of the self-potential data to the logarithm of the hydraulic conductivity, respectively. The technique followed in computing the two Jacobian matrices is detailed in section 3.1.

The optimization is done by following an iterative procedure according to [see *Kitanidis, 1996*]:

$$\tilde{\mathbf{s}}_{k+1} = \mathbf{X}\beta_{k+1} + \mathbf{QH}_k^T \xi_{k+1}, \quad (16)$$

where $\tilde{\mathbf{s}}_{k+1}$ denotes the updated best estimation of the vector of model parameter, and β_{k+1} and ξ_{k+1} are computed by solving the following linear system of equations:

$$\begin{pmatrix} \mathbf{H}_k \mathbf{QH}_k^T + \mathbf{V}_{h,\varphi} & \mathbf{H}_k \mathbf{X} \\ (\mathbf{H}_k \mathbf{X})^T & 0 \end{pmatrix} \begin{pmatrix} \xi_{k+1} \\ \beta_{k+1} \end{pmatrix} = \begin{pmatrix} \mathbf{d}_{h,\varphi}^{obs} - \Psi(\mathbf{s}_k) + \mathbf{H}_k \mathbf{s}_k \\ 0 \end{pmatrix}. \quad (17)$$

To estimate the uncertainty corresponding to the inverted field parameter, we compute the posterior covariance of \mathbf{s} , derived as:

$$\mathbf{Q}_{ss|d} = \mathbf{Q} - \begin{bmatrix} \tilde{\mathbf{H}}_k \mathbf{Q} \\ \mathbf{X}^T \end{bmatrix}^T \begin{pmatrix} \tilde{\mathbf{H}}_k \mathbf{QH}_k^T + \mathbf{V}_{h,\varphi} & \tilde{\mathbf{H}}_k \mathbf{X} \\ (\tilde{\mathbf{H}}_k \mathbf{X})^T & 0 \end{pmatrix}^{-1} \begin{bmatrix} \tilde{\mathbf{H}}_k \mathbf{Q} \\ \mathbf{X}^T \end{bmatrix}. \quad (18)$$

The diagonal elements of $\mathbf{Q}_{ss|d}$ represent the posterior variance of individual elements of $\tilde{\mathbf{s}}$. We pointed out that a line search algorithm is included in the optimization process to ensure that our new model update reduces adequately the objective function.

To visualize the quality of the coverage provided by the arrangements of the sources and receivers for a given case study and to quantify the nonuniqueness of the inversion, we compute the resolution matrix \mathbf{R} [Menke, 1989; Bohling and Butler, 2010]. This matrix is given by

$$\mathbf{R} = (\mathbf{H}_k^T \mathbf{V}^{-1} \mathbf{H}_k + \mathbf{M})^{-1} \mathbf{H}_k^T \mathbf{V}^{-1} \mathbf{H}_k, \quad (19)$$

where,

$$\mathbf{M} = \mathbf{Q}^{-1} - \mathbf{Q}^{-1} \mathbf{X} (\mathbf{X}^T \mathbf{Q}^{-1} \mathbf{X})^{-1} \mathbf{X}^T \mathbf{Q}^{-1}. \quad (20)$$

The matrix element R_{ij} denotes the weight contribution of the j th parameter to the estimate of the i th parameter. The values of the diagonal elements R_{ii} are comprised between 0 and 1. Zero means the parameter in question cannot be resolved at all given the data set while 1 means it can be perfectly resolved. Thus, the resolution matrix can be used to evaluate the effect of different sampling schemes of the pumping tests on the reconstruction of the hydraulic conductivity [Vasco et al., 1997].

3.1. Sensitivity Analysis

The application of a gradient-based algorithm involves an evaluation of the sensitivity matrix at each iteration. This computation represents the most computationally expensive part of the algorithm. The finite difference approach is a straightforward approach to determine the sensitivity matrix but nevertheless the computational effort is very high, especially when the number of the unknown parameters is important. An alternative approach is to apply the continuous adjoint-state method to reduce the cost for the computation of the sensitivity matrix [see *Sun and Yeh, 1990*].

For a given step in the iterative process of the quasi-linear algorithm in which $\tilde{\mathbf{s}}_k$ is the current estimate of the hydraulic conductivity $\tilde{K} = 10^{\tilde{\mathbf{s}}_k}$, we solved the hydroelectric forward problem to determine the distribution of the hydraulic head \tilde{h} and the streaming potential signature $\tilde{\varphi}$. Then, we solved a set of adjoint-state equations for each measurement. The sensitivity of φ to $\log \tilde{K}$ is given by satisfying the following two adjoint equations ψ_1^* and ψ_2^* :

$$-\nabla \cdot (\sigma \nabla \psi_1^*) = \delta(x - x_\phi^i), \quad (21)$$

$$\nabla \cdot (\tilde{K} \nabla \psi_2^*) = -\nabla \cdot \mathbf{j}^*, \quad (22)$$

with $\mathbf{j}^* = \alpha(\tilde{K}) \nabla \psi_1^*$, and

$$\alpha(\tilde{K}) = \hat{Q}_V(\tilde{K}) \tilde{K}. \quad (23)$$

These partial differential equations are subject to the following boundary conditions:

$$\psi_1^* = 0 \text{ at } \Gamma_D, \quad (24)$$

$$-\mathbf{n} \cdot [\sigma \cdot \nabla \psi_1^*] = 0 \text{ at } \Gamma_N, \quad (25)$$

$$\psi_2^* = 0 \text{ at } \Gamma_D, \quad (26)$$

$$-\mathbf{n} \cdot \tilde{K} \nabla \psi_2^* = 0 \text{ at } \Gamma_N, \quad (27)$$

where δ denotes the Dirac (delta) distribution, x is the spatial coordinates vector, and x_ϕ^i represents the position of the electrode at which measurement i is taken. The sensitivity of the self-potential measurements φ to the logarithm of the hydraulic conductivity $\tilde{\mathbf{s}} = \log_{10} \tilde{K}$ is then given as:

$$\frac{\partial \varphi_i}{\partial \tilde{\mathbf{s}}_k} = -\ln(10) \int_{\Omega_k} \left[\tilde{K} \nabla \tilde{h} \nabla \psi_2^* + \frac{\partial \alpha(\tilde{K})}{\partial \tilde{K}} \nabla \tilde{h} \nabla \psi_1^* \right] d\Omega_k. \quad (28)$$

The subscript k denotes the position of the unknown parameter $\tilde{\mathbf{s}}_k$ in the domain Ω . The subscript i denotes location of the self-potential observation.

A similar procedure is followed to evaluate the sensitivity of the hydraulic head measurements to the logarithm of the hydraulic conductivity data though by solving an equation for the adjoint-state ψ_3^* :

$$-\nabla \cdot (\tilde{K} \nabla \psi_3^*) = \delta(x - x_h^i), \quad (29)$$

subject to the following boundary conditions:

$$\psi_3^* = 0 \text{ at } \Gamma_D, \quad (30)$$

$$-\mathbf{n} \cdot \tilde{K} \nabla \psi_3^* = 0 \text{ at } \Gamma_N. \quad (31)$$

The sensitivity of h to $\mathbf{s} = \log_{10} K$ is then given as:

$$\frac{\partial h_i}{\partial \mathbf{s}_k} = -\ln(10) \int_{\Omega_k} \tilde{K} \nabla \tilde{h} \nabla \psi_3^* d\Omega_k. \quad (32)$$

The subscript k denotes the position of the parameter \mathbf{s}_k in the domain Ω while x_h^i denotes the location of the piezometric observation at position i . The integration of equations (28) and (32) is performed numerically with the Gauss-Legendre quadrature method.

Note that computing the sensitivity matrix using the finite differences method requires solving the forward problem $(n + 1)$ times in which n denotes the number of model parameters. This can become very tedious from a numerical standpoint if we are dealing with a high number of unknowns as this is the case. In addition, the use of adjoint operators gives a better estimate of the integral in equation (28) than the finite difference method.

4. Numerical Case Studies

We investigate now the usefulness of adding self-potential measurements to hydraulic head data simulated during pumping/injecting experiments to assess the hydraulic conductivity field of a 3-D heterogeneous

Table 1. Summary of Parameters Used to Construct the (True) Model in the Synthetic Examples^a

Dimensions	3-D
Geometry	10 m × 10 m × 4 m domain (cases 1–4) 40 m × 40 m × 40 m domain (case 5)
Number of nodes	48,690 (cases 1–4) 128,652 (case 5)
Number of parameter cells	392
HH Measurements error	HH Gaussian, $\sigma = 1$ cm in head
SP Measurements error	SP Gaussian, $\sigma = 0.1$ mV in voltage SP Gaussian, $\sigma = 0.08$ mV in voltage (case5)
Variogram for true $\log(K)$	$0.001 + 1 \text{ Gau}(60, 80, 0, 0, 0.66, 0.3)^b$
Variogram for true $\log(\sigma)$	$0.001 + 1 \text{ Gau}(300, 80, 0, 0, 0.6, 0.43)$

^aHH stands for hydraulic heads and SP for self potential (Case Studies 1–5).

^b $C_0 + C_1 \text{Gau}(a, p, q, r, s, t)$ where C_0 denotes the nugget, C_1 denotes the variance, a is the maximum range in the major direction, p, q is the dip angle for the principal direction of continuity, r is the third rotation angle to rotate the two minor directions around the principal direction defined by p and q . Anisotropy ratios s and t are the ratios between the major range and each of the two minor ranges. The error in the head data should account for both the uncertainty in the measurement of the head in the piezometer but also about the perturbation associated with the local disturbances in the K -field generated by the introduction of a piezometer in the ground.

aquifer. We propose five synthetic case studies in which we attempt to reproduce the hydraulic conductivity of a confined aquifer from the inversion of either the self-potential or the hydraulic heads data alone (case study 1), or through their joint inversion of these data (case studies 2–4). Case study 4 focuses on investigating the effect of the resistivity distribution known with some uncertainty. Case study 5 deals with a larger portion of an confined aquifer accounting for the finite thickness of the confining unit above the confined aquifer.

4.1. Synthetic Aquifer

The heterogeneous hydraulic conductivity field is geostatistically generated using the software SGEMS [Deutsch and Journel, 1992]. For that purpose, we use an anisotropic Gaussian variogram (see Table 1). The resulting hydraulic conductivity field is highly heterogeneous in XY directions and moderately heterogeneous in the Z direction. The values of the hydraulic conductivity are chosen to approximate a sandy alluvial environment (Figure 2a). The dimension of the area of interest is a square (10 m by 10 m) with thickness of 4 m (Figure 2a). The aquifer domain is encircled by a large area in which the electrical and hydraulic conductivities are constant to minimize the effect of boundary conditions chosen to solve the partial differential

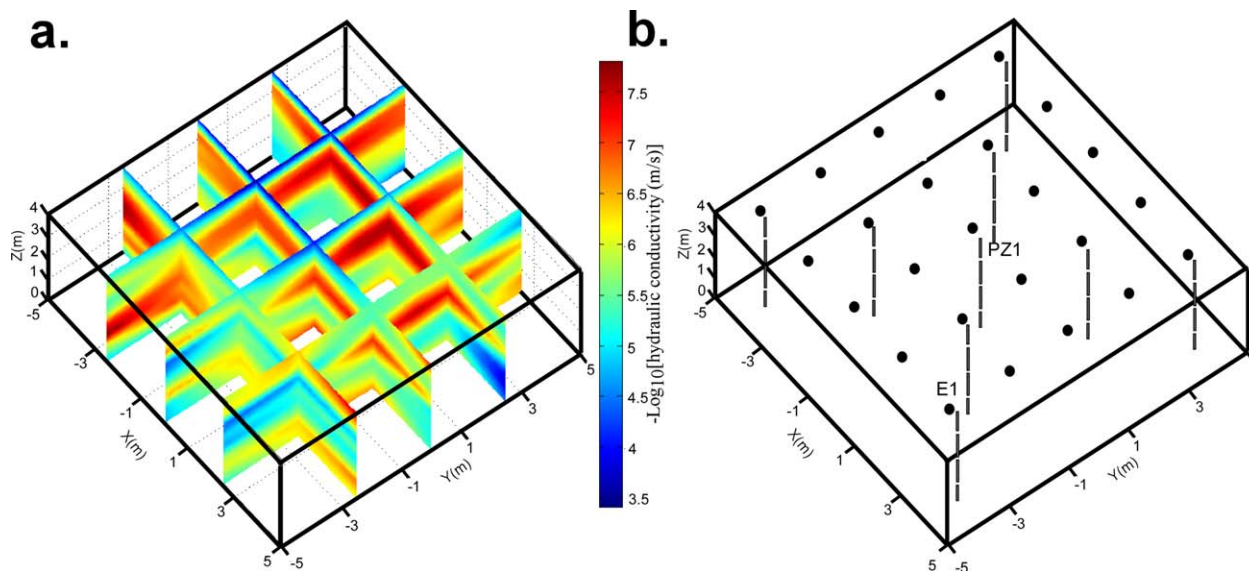


Figure 2. Description of the synthetic model. (a) True distribution of the hydraulic conductivity field generated by SGEMS [Deutsch and Journel, 1992]. This field is used to simulate the hydraulic heads and the self-potential data for a set of pumping tests. (b) Location of the nine wells used in case 1. This set of wells is used to simulate a sequence of pumping tests (pumping/injection at three discrete depth intervals (−3, −2, −1 m)) and to compute the hydraulic heads. The 25 filled circles on the top surface of the domain denote the position of the electrodes where the self-potential measurements are performed.

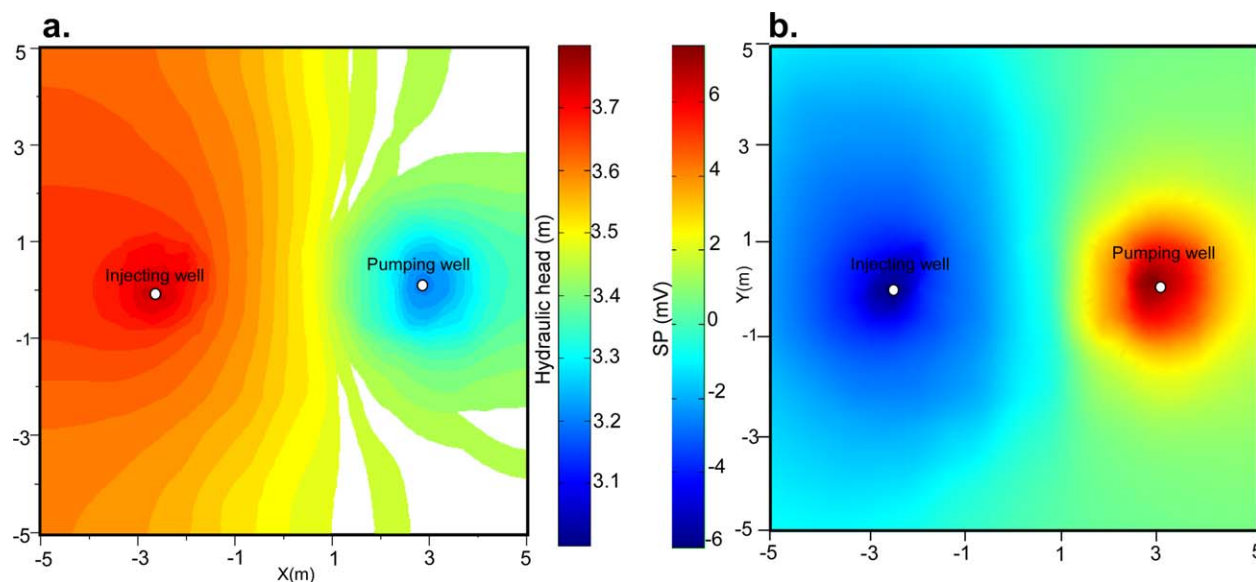


Figure 3. Distribution of heads (in the aquifer) and self potential (at the ground surface) for a single dipole test. (a) Distribution of the hydraulic heads (as meters above base datum) under steady state conditions. The filled circles correspond to the positions of located pumping and injecting wells. (b) Distribution of self potential at the ground surface corresponding to the hydraulic heads distribution in which the pumping and injecting zones characterized by the negative and positive signatures, respectively. Note that the magnitude of the self-potential signals is much above the typical noise level (0.1 mV) [e.g., Rizzo *et al.*, 2004].

equation of the electrical and hydraulic problems. The boundary Γ_D denotes the boundary at which the constant hydraulic head h_D is imposed. This boundary is located away from the domain of interest to ensure that the boundary conditions have no influence on the computation of the hydraulic heads. The Neumann boundary Γ_N is imposed at the surface and at the bottom of the domain of interest. The electrodes are located at the top aquifer/aquitard contact but they could be located further up and this will not change our results (see discussion below and see Figure 11 of Titov *et al.* [2005]).

The distribution of the electrical conductivity of the aquifer is assumed homogeneous only for case studies 1–3 (with $\sigma = 10^{-2} \text{ S m}^{-1}$) and heterogeneous in the fourth case. In this fourth case, we study the influence of the uncertainty of the electrical conductivity pattern on the result of the inversion of the self-potential data in terms of the hydraulic conductivity distribution. In the case of complex geological environments, an estimate of the electrical conductivity distribution can be derived independently from galvanometric or inductive electromagnetic methods. The efficiency of the hydraulic conductivity prediction from the pumping experiments depends on the number of piezometers and electrodes. We first investigate therefore three case studies with different densities of wells and electrodes in order to explore the potential benefits of including the self-potential data into the hydraulic tomography problem. As explained above, we only study the steady state conditions, that is for the self-potential signals, the difference in the electrical potential prior to the pumping tests and when the flow reaches a steady state equilibrium.

4.2. Case Study 1

In the first case study, we use nine wells considered to be packed off so that the head measurements and the pumping/injecting tests can take place at three discrete depth intervals $[-3, -2, \text{ and } -1 \text{ m}]$ (Figure 2b). Such a setup can be used to simulate a set of 324 hydraulic head data derived from 15 dipole tests (water is pumped in one well at one depth interval and injected into another one at various levels in the different wells). In parallel to the hydraulic head measurements, we also simulate the associated self-potential data at the ground surface of the domain using 25 electrodes with respect to a reference electrode placed 95 m away from the region of investigation (Figure 2b). The self-potential signals mimic the behavior of the hydraulic heads. The self-potential anomaly associated with the injection wells presents a negative signature and positive for the pumping wells (Figure 3) with a good signal-to-noise ratio as discussed below in section 5. Note that in real case studies, the temperature changes may cause drift in the self-potential

Table 2. Computed Mean Squared Deviations for Parameter Estimates (Estimated Versus True Values) and Data Residuals (Simulated Versus Observed) With the Number of the Iterations Needed to Reach the Convergence for Each Inversion^a

	Tests	Number of Data	MM ^b	DM ^c	Iterations
Case 1	HH	324	0.3885	0.0033	11
	SP	375	0.3882	0.0017	8
Case 2	HH	120	0.7310	0.0289	9
	SP	594	0.3899	0.0020	10
	HH + SP	120 + 594	0.3103	0.0066	8
Case 3	SP	375	0.8203	0.0008	7
Case 4	HH + SP (0% errors on σ)	120 + 594	0.3139	0.0020	10
	HH + SP (5% errors on σ)	120 + 594	0.4877	0.0485	11
	HH + SP(10% errors on σ)	120 + 594	0.7953	0.6120	6
Case 5	HH + SP	120+594	0.2603	0.0020	8

^aM and N denotes the number of model parameters and the number of data, respectively. HH and SP denote the hydraulic head and self-potential data, respectively.

^bMM denotes the model misfit defined by $MM = (1/M) \sum_{j=1}^M (s_{True} - s_{inverted})^2$.

^cDM denotes the data misfit defined by $DM = (1/N) \sum_{j=1}^N (d_{True} - d_{inverted})^2$, the data are either the hydraulic head data, or the absolute value of the self-potential data, or a combination of both.

temporal record. This drift needs to be removed/corrected prior analyzing the data (see details in *Jardani et al. [2009]*).

The hydraulic head data were contaminated with an artificial 5% Gaussian noise (using 5% of the mean of the hydraulic head data). This realistic level of noise is used to approximate real field conditions. We start the iterative process of our algorithm with a homogenous model of hydraulic conductivity $K = 10^{-6} \text{ m s}^{-1}$ for this inversion and also for the examples discussed below in this paper. The convergence was obtained in 11 iterations with an excellent fit for the hydraulic head observations (see Table 2). The inverted hydraulic conductivity field using the heads reproduces successfully the main pattern of the true *K*-field (see Figures 4a and 4b). This adequate estimate is due to the excellent spatial resolution associated with the use of a significant density of wells, which are well distributed in space to cover the heterogeneities of the aquifer. The sensitivity map obtained by the resolution matrix is shown in Figure 5a. It shows that the most sensitive regions are located close to the wells as expected.

In the next step, we examine the results of the inversion of the self-potential data associated with a set of dipole tests in the confined aquifer. A Gaussian random noise with a standard deviation of 5% of the mean value of the absolute value of the measurements was added to these data. The iterative inversion of the self-potential data starts also with a homogenous hydraulic conductivity model using $K = 10^{-6} \text{ m s}^{-1}$. The convergence was reached in eight iterations (see Table 2). The hydraulic conductivity tomography obtained from the inversion of the self-potential data can also be used to identify the major features of the hydraulic conductivity field (see Figures 4c and 4d). In order to explain the good result for the inversion of the self-potential data, we show the resolution matrix in Figure 5b. Good resolution is obtained close to the electrodes and a poor resolution is obtained at depth. This clearly indicates that the self-potential signals simulated at the ground surface are not very suitable to resolve vertical variations in the *K*-field.

Comparing the resolution maps of Figure 5a with Figure 5b, we can conclude that the head and self-potential data are complementary to each other in order to determine the distribution of the *K*-field. That said, there are still some areas in the aquifers that are poorly resolved by each of the method. Therefore, the joint inversion of the head and self-potential data should improve the determination of the *K*-field by comparison with using the head data alone. However, the joint inversion will still not be able to resolve the *K*-field in some area. In the next section, we analyze in what cases the self-potential signals could be advantageous in bringing useful information in the joint inversion problem.

4.3. Case Study 2

In the second case study, we reduced the number of wells to five and we increase the number of electrodes to 70. We simulated nine dipole tests and we obtained 120 hydraulic head data and 594 self-potential data (Figure 6). The hydraulic conductivity predicted by the inversion of hydraulic data is not able to delineate the true conductivity field of the aquifer (see Figures 7a and 7b and Table 2). This poor result is due to the

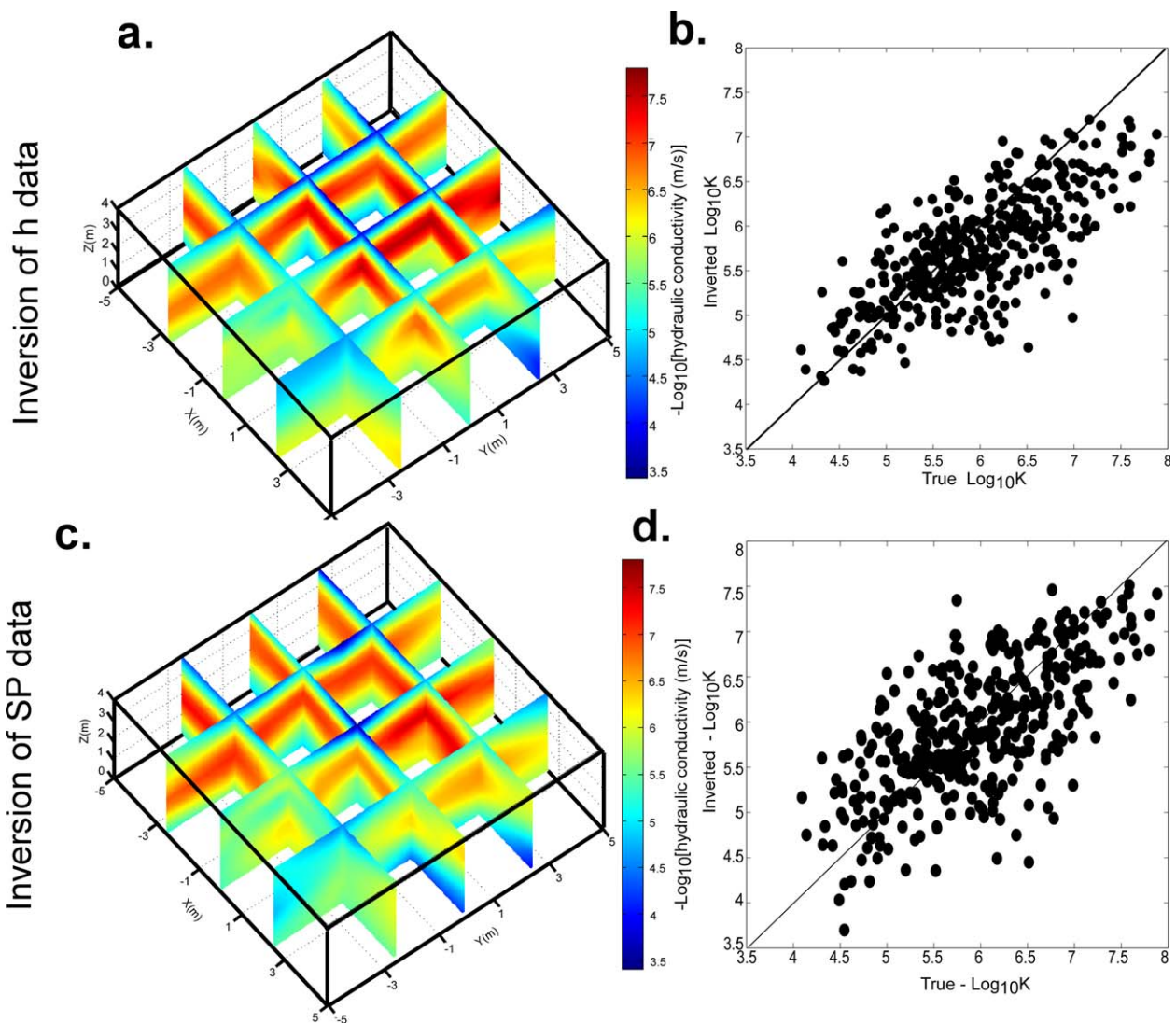


Figure 4. Results for case study 1. (a) Hydraulic conductivity field estimated from the inversion of the hydraulic head data simulated with the nine wells. (b) Comparison between the estimated and the true hydraulic conductivities. (c) Hydraulic conductivity field reconstructed from the inversion of the self-potential data. (d) Comparison between the estimated and the true hydraulic conductivities.

insufficient number of piezometers leading necessarily to a low resolution in the determination of the hydraulic conductivity field except in the areas close to the wells (Figure 8a).

The inverted hydraulic conductivity field obtained from the inversion of the self-potential data alone provide a better result than by using the hydraulic head data alone (see Figures 7c and 7d and Table 2 and compare with Figures 7a and 7b). This better performance is related to the higher density of electrodes in this case study. This high density improves the resolution of the hydraulic conductivity field as shown by the sensitivity map (Figure 8b). The self-potential signals are clearly very sensitive to the lateral variation in the hydraulic conductivity. These data capture the pattern of the heterogeneity around the wells even though it is a smooth estimation.

The next step is the joint inversion of the two sources of data. Because of the complementary nature of the sensitivity maps shown in Figure 8, we expect an improved determination of the K -field. This is indeed the case. The reconstructed hydraulic conductivity field honors the main heterogeneities shown in the true hydraulic conductivity field (see Figures 8c and 8d and Table 2 and compare with Figure 2). Therefore, the combination of the electrical and hydraulic data brings a significant improvement regarding the assessment of the hydraulic conductivity field. We can better delineate important preferential flow pathways.

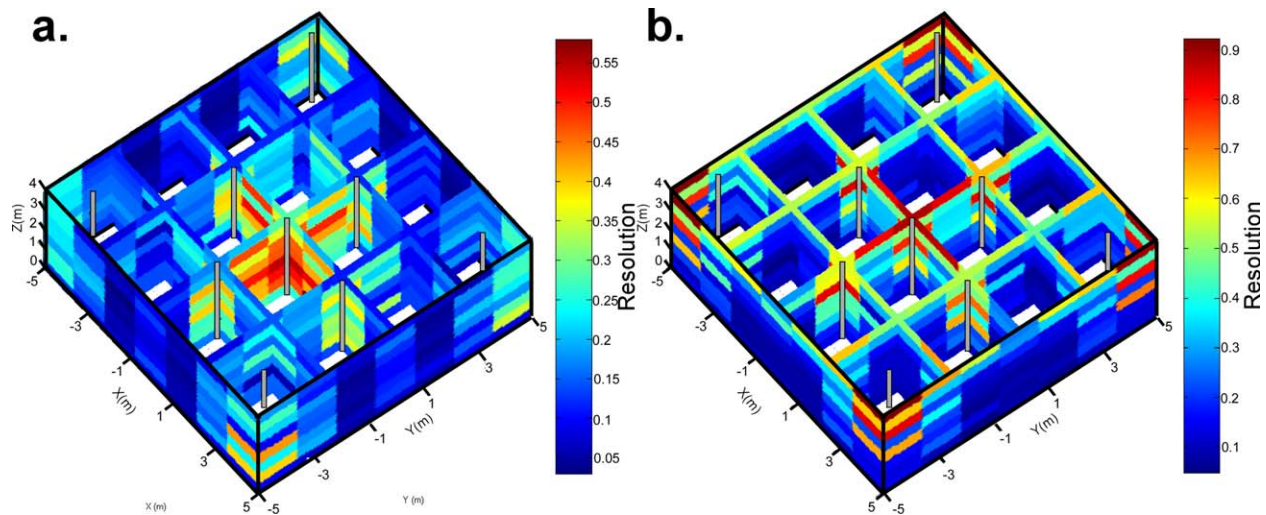


Figure 5. Case study 1. (a) Sensitivity of log of the hydraulic conductivity distribution to the hydraulic head. The sensitivity is high close to the piezometers and in the central part. (b) Sensitivity of log of the hydraulic conductivity distribution the self-potential data. There is a certain complementary between the two sensitivity maps but some regions are not resolved by the two techniques. We show the diagonal terms of the resolution matrix R. Values close to one indicate region that can be resolve nearly perfectly.

4.4. Case Study 3

In the third case study, we consider the case corresponding to a single piezometer and 70 electrodes. The pumping tests are performed at three different levels in the piezometer (Figure 9a). In this case, we simulated 189 self-potential measurements. The inversion of these self-potential data is used to invert the hydraulic conductivity field in the areas located around the well where the sensitivity is high (Figure 9b). However, a comparison between the real and inverted hydraulic conductivity fields shows that the reconstruction is over smooth (see Figures 9c and 9d and Table 2 and compare to Figure 2).

4.5. Case Study 4

In this case study, we go back to the same conditions used in case study 2 with 5 wells and 70 electrodes. We consider however that the distribution of the electrical resistivity of the aquifer is now heterogeneous

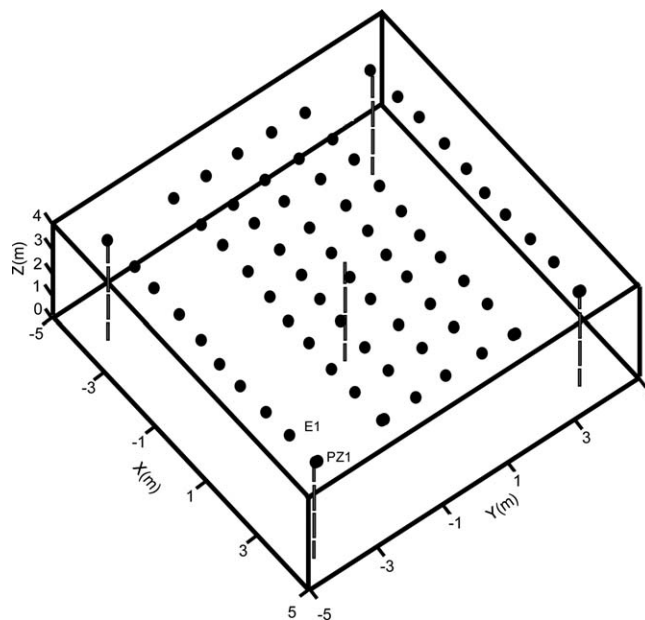


Figure 6. Case study 2. Position of the 5 wells and 70 electrodes used to simulate the synthetic observations that are then inverted to determine the hydraulic conductivity field.

because we are looking to evaluate the effect of the uncertainty in the electrical conductivity distribution on the estimate of the hydraulic conductivity. In this case study, we will jointly invert the head and self-potential data.

The heterogeneous distribution of the electrical conductivity is geostatistically generated using the software SGEMS [Deutsch and Journel, 1992], wherein the electrical conductivity varies within the following range: $[4 \times 10^{-4} \text{ S m}^{-1}; 5 \times 10^{-3} \text{ S m}^{-1}]$ giving a moderately heterogeneous field (Figure 10). This case mimics a fresh aquifer in terms of resistivity values. The electrical resistivity is not related anyhow to the K-field except on the observed fact (well explained by petrophysical models) that the

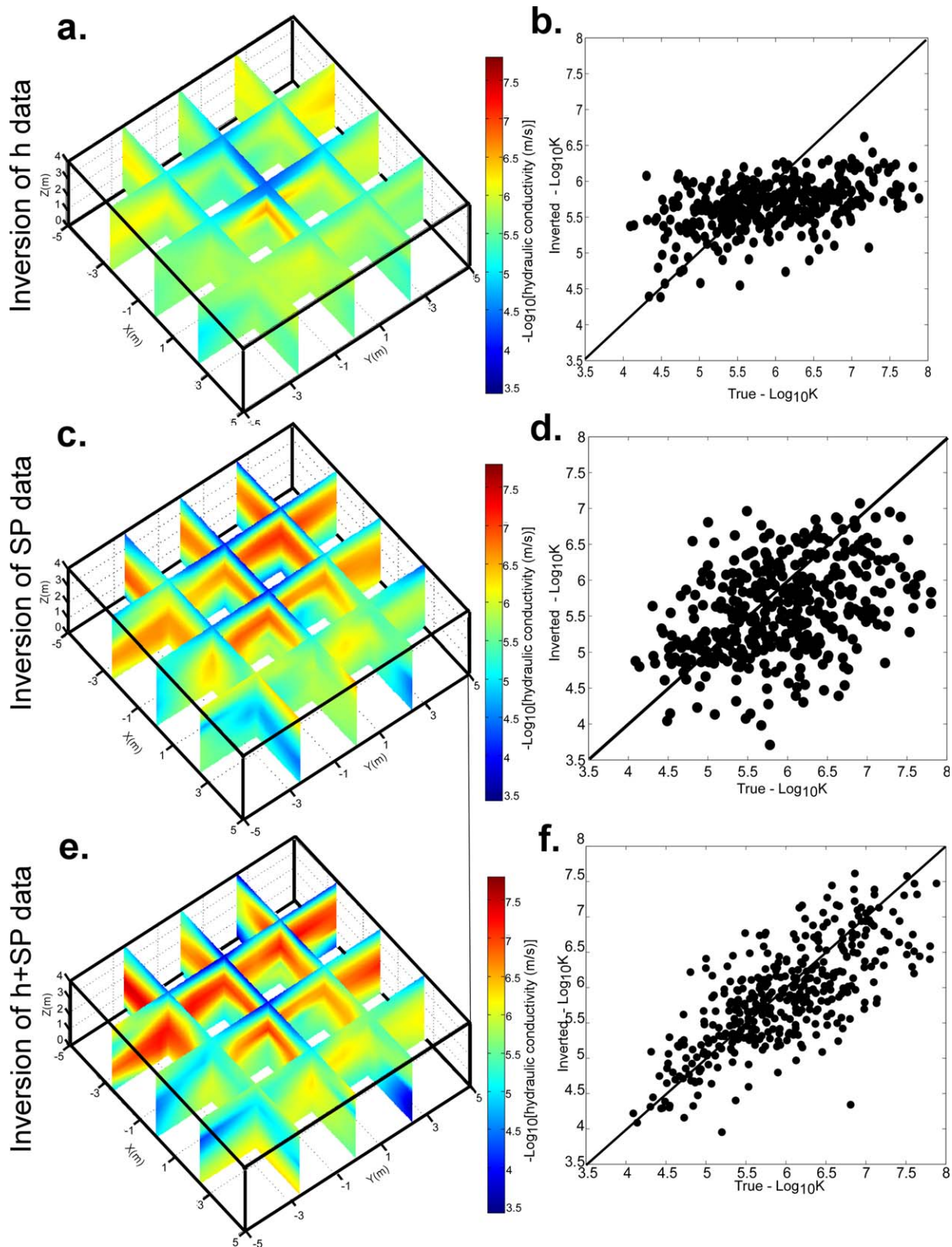


Figure 7. Case study 2. (a) Hydraulic conductivity field estimated from the inversion of the hydraulic head data. (b) Comparison between the estimated and the true hydraulic conductivities. (c) Hydraulic conductivity field inferred from the inversion of the self-potential data. (d) Comparison between the estimated and the true hydraulic conductivities. (e) Hydraulic conductivity field inferred from the joint inversion of the self-potential data and the hydraulic head data. (f) Comparison between the estimated and the true hydraulic conductivities for the joint inversion problem. We see clearly an improvement of the inversion results by adding the self-potential data to the hydraulic data.

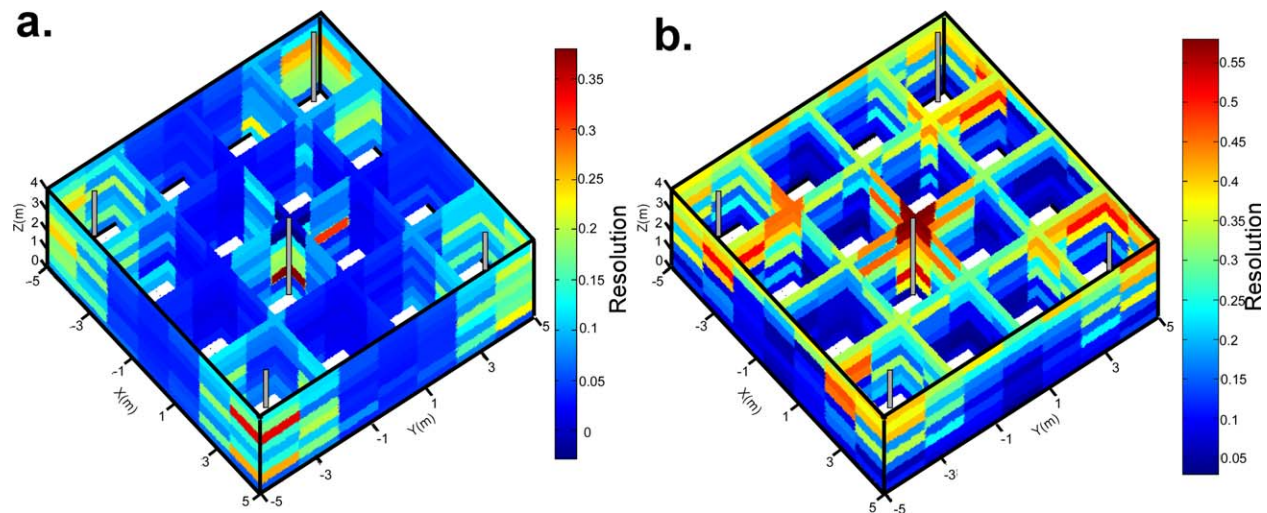


Figure 8. Case study 2. (a) Sensitivity map for the log of the hydraulic conductivity to the hydraulic head. (b) Sensitivity map for the log of the hydraulic conductivity to the self-potential data. In this case, we see the value of the self-potential signals in helping the inversion to converge to a better hydraulic conductivity field.

resistivity field has a variance that is always much smaller than the variance associated with the K -field. In this case study, we consider three distinct tests for the joint inversion with each time a distinct level of knowledge about the electrical conductivity distribution of the aquifer.

In the first test, we assume that the distribution of the electrical conductivity is completely known, so the joint inversion is carried out with the distribution of electrical conductivity used to simulate the self-potential data. The result of the joint inversion honors the main heterogeneity of the hydraulic conductivity (Figures 11a and 11b). In the second test, the electrical conductivity introduced in the joint inversion is contaminated with a Gaussian random noise with a standard deviation of 5% of the mean value of the electrical conductivity of the field. The result provides an acceptable characterization of the hydraulic conductivity of the aquifer, but we observe a clear increase in the degree of uncertainty of the reconstruction compared to the first test (compare Figures 11c and 11d with Figures 11a and 11b).

In the third test, we increase again the degree of uncertainty associated to the electrical conductivity distribution using a standard deviation reaching 10% of the mean value of the electrical conductivity. In this case, we observe that the inverted K -field loses its reliability (Figures 11e and 11f). We conclude therefore that the reconstruction of the hydraulic conductivity from the self-potential data depends on the knowledge of the distribution of the electrical conductivity. Therefore self-potential monitoring of pumping tests should be accompanied by electrical resistivity tomography and new strategies should be developed to improve the resolution of resistivity tomography for such cases (note that in some cases, GPR may be used to bring a high-resolution resistivity tomography [e.g., Lavoué *et al.*, 2014]), that could be used in turn in the self-potential inverse problem.

4.6. Case Study 5

In this case study, we model a larger portion of an aquifer covering an area of 40×40 m (thickness 30 m) with an explicit modeling of the confining unit with a thickness of 10 m. The 63 electrodes are located at the ground surface at a depth of 40 m. We consider five piezometers at the following positions P1 ($x = -16$ m, $y = 16$ m), P2 ($x = -16$ m, $y = -16$ m), P3 ($x = 0$, $y = 0$), P4 ($x = 16$ m, $y = -16$ m), and P5 ($x = 16$ m, $y = 16$ m). The heads are taken at three levels for each piezometer: 10, 20, and 28 m. The position of the electrodes and piezometers is the same as in Figure 6. The electrical conductivity of the confining unit is 10^{-3} S m^{-1} and its hydraulic conductivity is 10^{-7} m s^{-1} .

The results of the inversion are shown in Figure 12. Figure 12a shows the true distribution of the K -field. Figure 12b shows the distribution of electrical conductivity, which is assumed to be perfectly known in this case study. The hydraulic conductivity field inferred from the joint inversion of the self-potential data and the hydraulic head data is shown in Figure 12c. We see that the distribution of the inferred K -field look very similar to the true distribution shown in Figure 12a. Because the electrodes are now further away from the

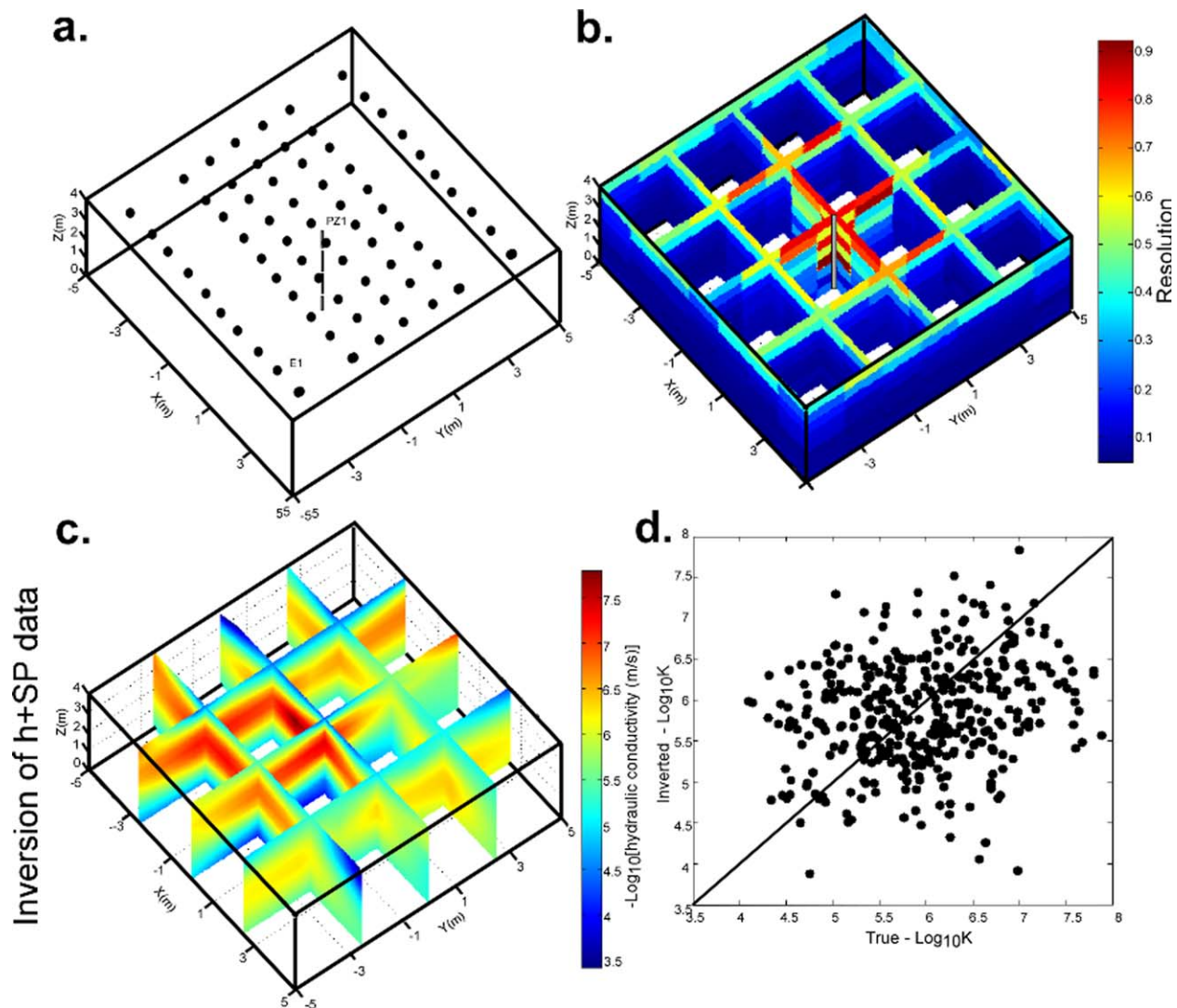


Figure 9. Case study 3. (a) Position of the unique well used for the pumping test and the electrodes. (b) Hydraulic conductivity resolution associated with the self-potential data. Note the lack of sensitivity with depth. (c) Hydraulic conductivity field estimated from the inversion of the self-potential data alone simulated during the pumping test performed with a single well. (d) Comparison between the estimated and the true values of the K -field.

volume in which groundwater flow occurs, it is expected that the reconstructed distribution of the K -field will be a bit smoother. Finally, Figure 12d shows a comparison between the estimated and the true hydraulic conductivities for the joint inversion problem. The reconstruction is rather good.

4.7. Convergence

Table 2 shows the data and model misfits for the different case studies and simulations. We see that the residual errors are small and that convergence of the algorithm is very fast, both for the inversion of the independent data sets (hydraulic heads or self-potential data) and for the joint inversion cases. We generally reach convergence in 6–11 iterations for all the investigated cases.

5. Discussion

There are few points that need to be discussed in this section. The first point concerns the signal-to-noise ratio of the self-potential method in field conditions. We will also discuss the impact of the uncertainty in the relationship between \hat{Q}_V and K on the uncertainty in the determination of the K -field. We will also

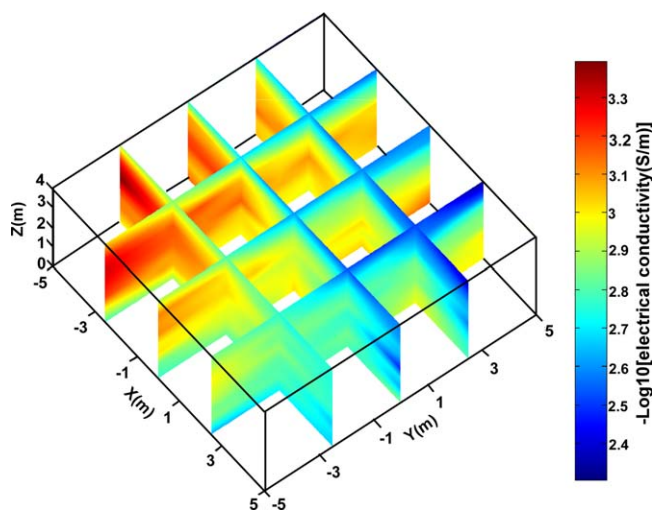


Figure 10. Spatial distribution of the electrical conductivity field used in case study 4.

discuss the impact of the resistivity distribution regarding the determination of the K -field. Finally, we will discuss the depth of the self-potential method to monitor pumping tests.

Concerning the signal-to-noise ratio of the self-potential measurements, in field conditions, the stability of the nonpolarizing electrodes remains an important issue especially the temperature dependence of the electrodes themselves (for instance, the potential of Cu/CuSO_4 is $1.6 \text{ mV}/^\circ\text{C}$). This temperature dependence may be responsible for the drift in the self-potential records if the scanning electrodes and the reference electrode experience dif-

ferent changes in temperature over time [see *Jardani et al.*, 2009]. Various approaches can be used to compensate for these effects as discussed by *Jardani et al.* [2009]. A second source of noise is the 60 Hz (or 50 Hz and their harmonics) that can be present in the time series. The simplest way to remove these signals is to use a Fourier transform of the drift-compensated signals and to use notch filter on the 60 Hz and its harmonic and then to come back to the time domain using an inverse Fourier transform (see, for instance, the field examples of *Buttler and Russel* [2003]). Other potentials sources of noise are discussed in *Revil and Jardani* [2013]. Once the raw data have been corrected for these problems, the noise level can be brought to 0.1–0.2 mV as shown by *Jardani et al.* [2009]. Consequently, the signal-to-noise ratio shown by synthetic data in Figure 3b is expected to be realistic. Note that the self-potential data that need to be considered in the inversion are the difference between the values measured prior the pumping tests and the values in steady state condition of flow. This point has been discussed in several papers, for instance, *Rizzo et al.* [2004], *Suski et al.* [2006], and *Straface et al.* [2010].

The second point to discuss is the uncertainty associated with the scatter shown in Figure 1. In our analysis, we have considered that equation (6) is certain while obviously this is not the case. That said, most of the scatter of the relationship in Figure 1 comes from the effect of salinity of the pore water. Because the salinity effect or the effect of the composition of the pore water upon the streaming potential coupling coefficient or the effective charge density can be estimated (see discussion in *Lorne et al.* [1999] and *Ikard et al.* [2012]), the scatter can be reduced by measuring the conductivity of the pore water (corrected for temperature). Another approach is to recognize such uncertainty explicitly in equation (6) and to use, for instance, a sequential Bayesian approach to determine its impact on the uncertainty of the inferred hydraulic conductivity field.

The third point concerns the resistivity distribution. For simplicity, we have considered a uniform electrical conductivity distribution for the three first case studies. However, we know that the electrical conductivity distribution can be heterogeneous with the possibility of some correlation in the spatial distribution of the electrical and hydraulic conductivities. As discussed in case study 4, the electrical conductivity directly impacts the value of the self-potential signals simulated at the ground surface [e.g., *Suski et al.*, 2006]. Thus, the proposed approach necessitates the determination of the distribution of the electrical conductivity. Various methods have been recently developed to image jointly the hydraulic conductivity and electrical conductivity (e.g., from GPR data) and using, for instance, structural similarities between the two distributions [*Lochbühler et al.*, 2013], or an inversion based on the cross-gradient approach [*Gallardo and Meju*, 2003]. A solution to this issue is to jointly invert hydraulic heads together with a combination of geophysical methods including DC resistivity (possibly induced polarization), GPR, and self-potential data.

The last point to discuss concerns the depth of investigation of the method. While defining a depth of investigation per se is meaningless for a passive potential field technique, it is legitimate to wonder to what

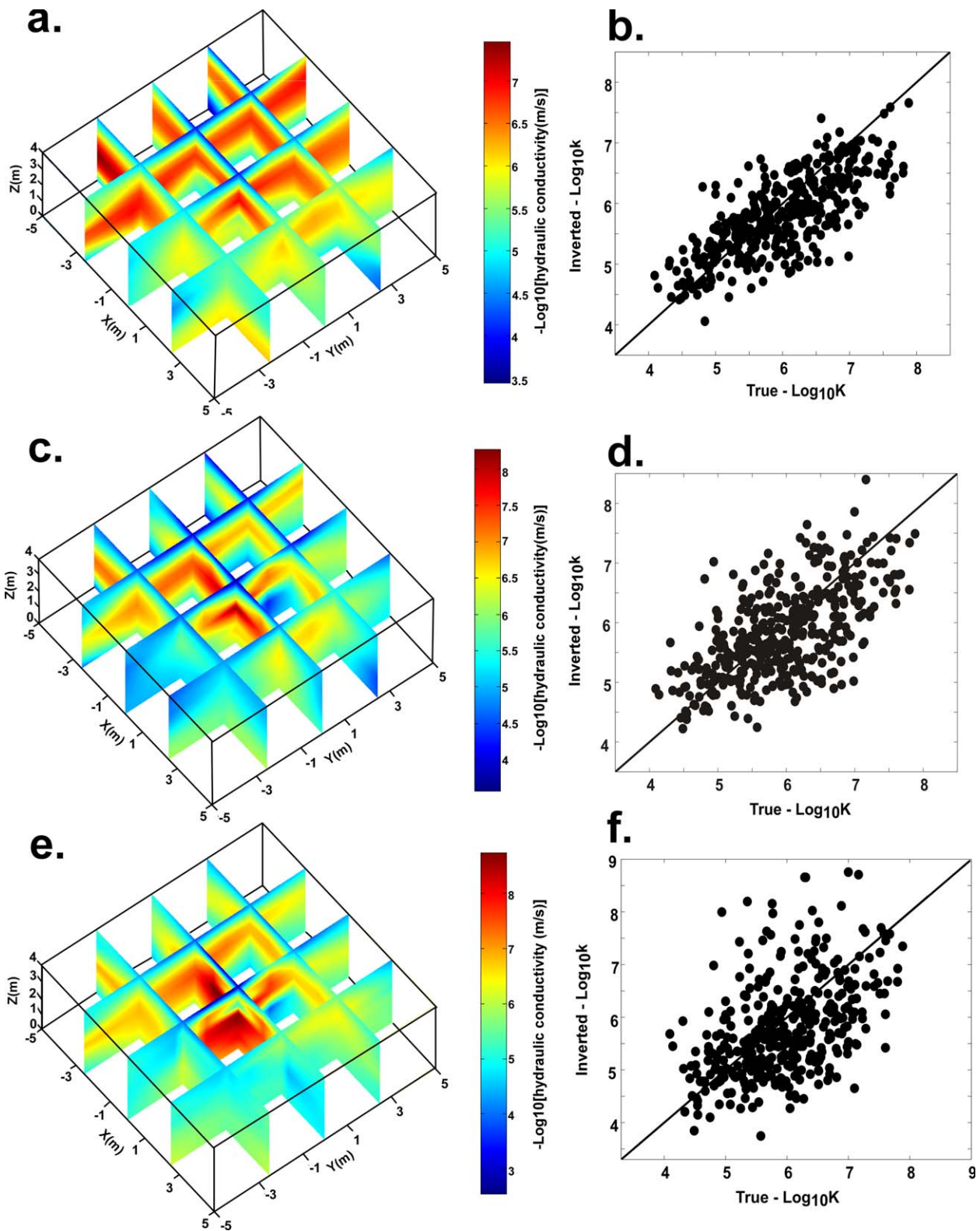


Figure 11. Case study 4. Three tests of the joint inversion of the hydraulic head and self-potential data (heterogeneous electrical conductivity field). (a) K -field estimated with the complete knowledge of the electrical conductivity distribution. (b) Inverted versus true hydraulic conductivity values. (c) Hydraulic conductivity estimated with a distribution of the electrical conductivity contaminated with a Gaussian random noise with a standard deviation of 5% of the mean value of the electrical conductivity of the field. (d) Inverted versus true hydraulic conductivity values. (e) Hydraulic conductivity estimated with a distribution of the electrical conductivity contaminated with a Gaussian random noise with a standard deviation of 10% of the mean value of the electrical conductivity of the field. (f) Inverted versus true hydraulic conductivity values.

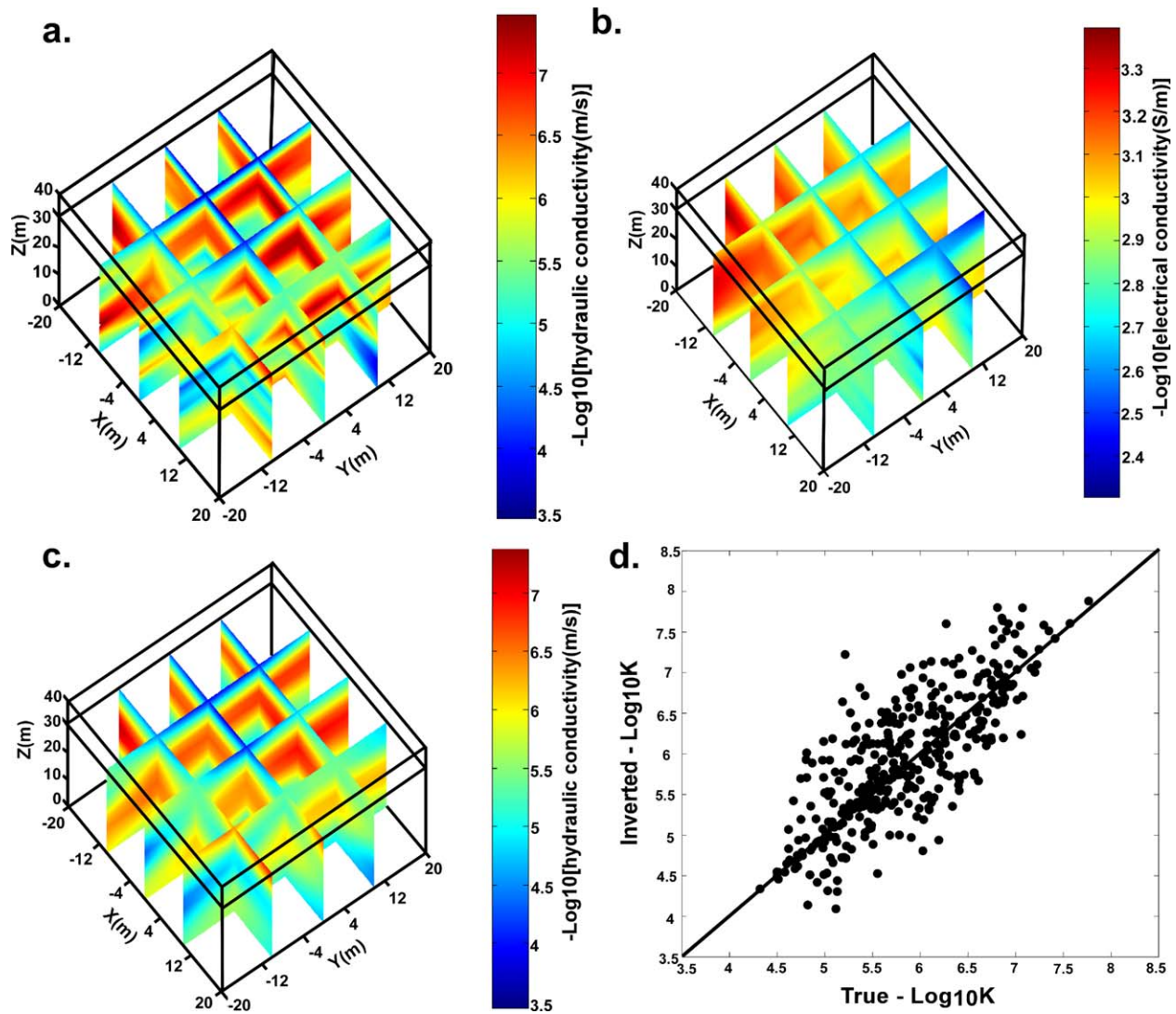


Figure 12. Case Study 5. (a) True distribution of the hydraulic conductivity field. (b) Distribution of electrical conductivity field. (c) Hydraulic conductivity field inferred from the joint inversion of the self-potential data and the hydraulic head data. (d) Comparison between the estimated and the true hydraulic conductivities for the joint inversion problem.

depth we can use the self-potential method to “feel” hydraulic head changes. In the case, where there is not a very conductive layer between the confined aquifer and the ground surface, we expect to have the equipotentials to be more or less normal to the aquifer/aquitard interface and to the ground surface (see, for instance, Figure 11 from *Titov et al.* [2005]). In this case, we expect to see reasonably well the effect of hydraulic head changes in a confined aquifer down to several tens of meters and possibly 100 m. Of course, it will be always good to perform some forward modeling using the state-of-knowledge of the resistivity distribution at a given site. In our cases, the upper confining layer extends to the surface and thus that no other sources of self-potential signal exists, e.g., from a perched aquifer. That said, even if there is source of electrical current associated with flow in a perched or unconfined aquifer, this is not a problem. Indeed, the electrical field associated with these sources can be easily removed by taking the reference self-potential distribution prior pumping and using only the time changes in the self-potential signals.

Our work can be applied to confined and unconfined aquifers [see *Malama et al.*, 2009a, 2009b]. We think that the next step will be to perform well-controlled sandbox experiments as done for hydraulic tomography by Walter Illman and coworkers [*Illman et al.*, 2007, 2010]. Preliminary works have been performed for unconfined aquifers by *Suski et al.* [2004] and *Straface et al.* [2010] but these works ignored the complications associated with the flow in the vadose zone. Recent modeling of the streaming current generated in

unsaturated media [Linde et al., 2007; Vinogradov and Jackson, 2011; Jougnot et al., 2012; Revil and Mahardika, 2013] makes it possible to simulate the effect of flow in the vadose zone under transient conditions. This is a problem that will require further investigations.

6. Conclusion

We are continually searching for better ways of characterizing the structure and magnitude of hydraulic conductivity in the shallow subsurface. The present work explores the potential value of using measurements of natural voltage patterns called self-potential signals along with hydraulic head data during pumping tests to infer the hydraulic conductivity field. Previous works have demonstrated that measurable electrical potential fluctuations can be measured for pumping/injection tests in shallow (<100 m) confined and unconfined aquifers. We have developed a method based on the adjoint-state approach to jointly invert hydraulic head and self-potential data. Five synthetic case studies have been tested to investigate the usefulness of adding self-potential measurements to hydraulic head data in order to reconstruct the hydraulic conductivity field of a heterogeneous aquifer during pumping tests.

In the presence of a few wells, the use of self-potential data improves significantly the determination of the hydraulic conductivity field. The self-potential signals measured at the ground surface are more sensitive to lateral variation of the hydraulic conductivity than to vertical variations. The resolution of the method decreases with the depth of the aquifer since the self-potential method belongs to the family of potential field problems. Our modeling tests reveal the importance of knowledge of the electrical conductivity distribution on the recovery of the K -field. Consequently future studies will need also to incorporate the resistivity information in the inverse problem and to extend the present approach to harmonic pumping tests.

Acknowledgments

We thank "Agence de l'Eau de Haute-Normandie" (France), "La Maison de l'Estuaire," and GPMH for funding the project "Hydromar." A.R. thanks the funding from NSF for the SmartGeo Educational Program (Project IGERT: Intelligent Geosystems; DGE-0801692) and the PIRE project. We thank the Editor, Harihar Rajaram, and the Associate Editor, Andrew Binley, for handling our manuscript and the pertinent and constructive reviews of Michael Cardiff, and three anonymous referees. The numerical data used in this manuscript can be obtained upon request to the authors and will be placed in ResearchGate.

References

- Abaza, M. M., and C. G. Clyde (1969), Evaluation of the rate of flow through porous media using electrokinetic phenomena, *Water Resour. Res.*, 5(2), 470–483.
- Ahmad, M. U. (1969), A laboratory study of streaming potentials, *Geophys. Prospect.*, 12(1), 49–64.
- Bachmetjew, P. I. (1896), *Hauptresultate der Untersuchungen über die Abhängigkeit der elektrischen Erdströme von Nibeau-Schwankungen des Grundwassers in Bulgarien*, vol. 4, pp. 300, Göttingen Nachrichten, Göttingen, Germany.
- Bear, J. (1988), *Dynamics of Fluids in Porous Media*, Dover, New York.
- Bogoslovsky, V. A., and A. A. Ogilvy (1973), Deformations of natural electric fields near drainage structures, *Geophys. Prospect.*, 21, 716–723.
- Bohling, G. C., and J. Butler (2010), Inherent limitations of hydraulic tomography, *Ground Water*, 48, 809–824.
- Bolève, A., A. Crespy, A. Revil, F. Janod, and J. L. Mattiuzzo (2007), Streaming potentials of granular media: Influence of the Dukhin and Reynolds numbers, *J. Geophys. Res.*, 112, B08204, doi:10.1029/2006JB004673.
- Bowling, J. C., C. M. Zheng, A. B. Rodriguez, and D. L. Harry (2006), Geophysical constraints on contaminant transport modeling in a heterogeneous fluvial aquifer, *J. Contam. Hydrol.*, 85, 72–88.
- Brauchler, R., R. Hu, L. Hu, S. Jiménez, P. Bayer, P. Dietrich, and T. Ptak (2013), Rapid field application of hydraulic tomography for resolving aquifer heterogeneity in unconsolidated sediments, *Water Resour. Res.*, 49, 2013–2024, doi:10.1002/wrcr.20181.
- Butler, K. E., and R. D. Russell (2003), Cancellation of multiple harmonic noise series in geophysical records, *Geophysics*, 68(3), 1083–1090.
- Cardiff, M., W. Barrash, P. K. Kitanidis, B. Malama, A. Revil, S. Straface, and E. Rizzo (2009), A potential-based inversion of unconfined steady-state hydraulic tomography, *Ground Water*, 47(2), 259–270, doi:10.1111/j.1745-6584.2008.00541.x.
- Cardiff, M., W. Barrash, and P. K. Kitanidis (2012), A field proof-of-concept of aquifer imaging using 3D transient hydraulic tomography with temporarily-emplaced equipment, *Water Resour. Res.*, 48, W05531, doi:10.1029/2011WR011704.
- Casagrande, L. (1983), Stabilization of soils by means of electro-osmosis: State of art, *J. Boston Soc. Civ. Eng.*, 69(2), 255–302.
- Chapman, D. L. (1913), A contribution to the theory of electrocapillarity, *Philos. Mag.*, 25(6), 475–481.
- Chen, J., S. S. Hubbard, and Y. Rubin (2001), Estimating the hydraulic conductivity at the South Oyster Site from geophysical tomographic data using Bayesian techniques based on the normal linear regression model, *Water Resour. Res.*, 37(6), 1603–1613.
- Deutsch, C., and A. Journel (1992), *GSLIB: Geostatistical Software Library and User's Guide*, Oxford Univ. Press, New York.
- Friberg, J. (1996), Experimental and theoretical investigations into the streaming potential phenomenon with special reference to applications in glaciated terrain, PhD thesis, Luleå Univ. of Technol., Luleå, Sweden.
- Gallardo, L. A., and M. A. Meju (2003), Characterization of heterogeneous near-surface materials by joint 2D inversion of DC resistivity and seismic data, *Geophys. Res. Lett.*, 30(13), 1658, doi:10.1029/2003GL017370.
- Gouy, G. L. (1910), Sur la constitution de la charge électrique à la surface d'un électrolyte, *J. Phys. Théor. Appl.*, 9(4), 457–468.
- Helmholtz, H. (1879), Study concerning electrical boundary layers, *Weidemann Ann. Phys. Chem.*, 7, 337–382.
- Hernandez, A. F., S. P. Neuman, A. Guadagnini, and J. Carrera (2006), Inverse stochastic moment analysis of steady state flow in randomly heterogeneous media, *Water Resour. Res.*, 42, W05425, doi:10.1029/2005WR004449.
- Hördt, A., R. Blaschek, A. Kemna, and N. Zisser (2006), Hydraulic conductivity estimation from induced polarisation data at the field scale: The Krauthausen case history, *J. Appl. Geophys.*, 62, 33–46.
- Hyndman, D. W., J. M. Harris, and S. M. Gorelick (2000), Inferring the relation between seismic slowness and hydraulic conductivity in heterogeneous aquifers, *Water Resour. Res.*, 36(8), 2121–2132.
- Ikard, S. J., A. Revil, A. Jardani, W. F. Woodruff, M. Parekh, and M. Mooney (2012), Saline pulse test monitoring with the self-potential method to non-intrusively determine the velocity of the pore water in leaking areas of earth dams and embankments, *Water Resour. Res.*, 48, W04201, doi:10.1029/2010WR010247.

- Illman, W. A., X. Y. Liu, and A. Craig (2007), Steady-state hydraulic tomography in a laboratory aquifer with deterministic heterogeneity: Multimethod and multiscale validation of hydraulic conductivity tomograms, *J. Hydrol.*, *341*(3–4), 222–234, doi:10.1016/j.jhydrol.2007.05.011.
- Illman, W. A., J. F. Zhu, A. J. Craig, and D. T. Yin (2010), Comparison of aquifer characterization approaches through steady state groundwater model validation: A controlled laboratory sandbox study, *Water Resour. Res.*, *46*, W04502, doi:10.1029/2009WR007745.
- Jardani, A., and A. Revil (2009), Stochastic joint inversion of temperature and self-potential data, *Geophys. J. Int.*, *179*, 640–654, doi:10.1111/j.1365-246X.2009.04295.x.
- Jardani, A., A. Revil, and J.-P. Dupont (2006), Self-potential tomography applied to the determination of cavities, *Geophys. Res. Lett.*, *33*, L13401, doi:10.1029/2006GL026028.
- Jardani, A., A. Revil, A. Bolève, A. Crespy, J.-P. Dupont, W. Barrash, and B. Malama (2007), Tomography of the Darcy velocity from self-potential measurements, *Geophys. Res. Lett.*, *34*, L24403, doi:10.1029/2007GL031907.
- Jardani, A., A. Revil, W. Barrash, A. Crespy, E. Rizzo, S. Straface, M. Cardiff, B. Malama, C. Miller, and T. Johnson (2009), Reconstruction of the water table from self-potential data: A Bayesian approach, *Ground Water*, *47*(2), 213–227, doi:10.1111/j.1745-6584.2008.00513.x.
- Jougnot, D., N. Linde, A. Revil, and C. Doussan (2012), Derivation of soil-specific streaming potential electrical parameters from hydrodynamic characteristics of partially saturated soils, *Vadoze Zone J.*, *11*(1), 272–286, doi:10.2136/vzj2011.0086.
- Kitanidis, P. K. (1996), On the geostatistical approach to the inverse problem, *Adv. Water Resour.*, *19*(6), 333–342.
- Kuhlman, K. L., A. C. Hinnell, P. K. Mishra, and T.-C. J. Yeh (2008), Basin-scale transmissivity and storativity estimation using hydraulic tomography, *Ground Water*, *46*(5), 706–715, doi:10.1111/j.1745-6584.2008.00455.x.
- Kulesa, B., B. Hubbard, and H. Brown (2003), Cross-coupled flow modeling of coincident streaming and electrochemical potentials, and application to subglacial self-potential (SP) data, *J. Geophys. Res.*, *108*(B8), 2381, doi:10.1029/2001JB1167.
- Lavoué, F., R. Brossier, L. Métivier, S. Garambois, and J. Virieux (2014), Two-dimensional permittivity and conductivity imaging by full waveform inversion of multioffset GPR data: A frequency-domain quasi-Newton approach, *Geophys. J. Int.*, *197*(1), 248–268, doi:10.1093/gji/ggt528.
- Linde, N., D. Jougnot, A. Revil, S. K. Matthai, T. Arora, D. Renard, and C. Doussan (2007), Streaming current generation in two-phase flow conditions, *Geophys. Res. Lett.*, *34*, L03306, doi:10.1029/2006GL028878.
- Liu, S., T.-C. J. Yeh, and R. Gardiner (2002), Effectiveness of hydraulic tomography: Sandbox experiments, *Water Resour. Res.*, *38*(4), 1034, doi:10.1029/2001WR000338.
- Liu, X., W. A. Illman, A. J. Craig, J. Zhu, and T.-J. Yeh (2007), Laboratory sandbox validation of transient hydraulic tomography, *Water Resour. Res.*, *43*, W05404, doi:10.1029/2006WR005144.
- Lochbühler, T., J. Doetsch, R. Brauchler, and N. Linde (2013), Structure-coupled joint inversion of geophysical and hydrological data, *Geophysics*, *78*(3), ID1–ID14, doi:10.1190/geo2012-0460.1.
- Lorne, B., F. Perrier, and J.-P. Avouac (1999), Streaming potential measurements. 1: Properties of the electrical double layer from crushed rock samples, *J. Geophys. Res.*, *104*(B8), 17,857–17,877, doi:10.1029/1999JB900156.
- Maineult, A., E. Strobach, and J. Renner (2008), Self-potential signals induced by periodic pumping tests, *J. Geophys. Res.*, *113*, B01203, doi:10.1029/2007JB005193.
- Malama, B. (2014), Theory of transient streaming potentials in coupled unconfined aquifer-unsaturated zone flow to a well, *Water Resour. Res.*, *50*, doi:10.1002/2013WR014909, in press.
- Malama, B., A. Revil, and K. L. Kuhlman (2009a), A semi-analytical solution for transient streaming potentials associated with confined aquifer pumping tests, *Geophys. J. Int.*, *176*, 1007–1016, doi:10.1111/j.1365-246X.2008.04014.x.
- Malama, B., K. L. Kuhlman, and A. Revil (2009b), Theory of transient streaming potentials associated with axial-symmetric flow in unconfined aquifers, *Geophys. J. Int.*, *179*, 990–1003, doi:10.1111/j.1365-246X.2009.04336.x.
- Mao, D., T.-C. J. Yeh, L. Wan, J.-C. Wen, W. Lu, C.-H. Lee, and K.-C. Hsu (2013), Joint interpretation of sequential pumping tests in unconfined aquifers, *Water Resour. Res.*, *49*, 1782–1796, doi:10.1002/wrcr.20129.
- Menke, W. (1989), *Geophysical Data Analysis: Discrete Inverse Theory*, Academic, San Diego, Calif.
- Pengra, D. S., S. X. Li, and P. Wong (1999), Determination of rock properties by low-frequency AC electrokinetics, *J. Geophys. Res.*, *104*(B12), 485–508, doi:10.1029/1999JB900277.
- Petiau, G. (2000), Second generation of lead-lead chloride electrodes for geophysical applications, *Pure Appl. Geophys.*, *3*, 357–382.
- Petiau, G., and A. Dupis (1980), Noise, temperature coefficient and long time stability of electrodes for telluric observations, *Geophys. Prospect.*, *28*(5), 792–804.
- Pollock, D., and O. A. Cirpka (2010), Fully coupled hydrogeophysical inversion of synthetic salt tracer experiments, *Water Resour. Res.*, *46*, W07501, doi:10.1029/2009WR008575.
- Quincke, G. (1859), Concerning a new type of electrical current, *Ann. Phys. Chem.*, *107*, 1–47.
- Revil, A. (2013), Effective conductivity and permittivity of unsaturated porous materials in the frequency range 1 mHz–1GHz, *Water Resour. Res.*, *49*, 306–327, doi:10.1029/2012WR012700.
- Revil, A., and N. Florsch (2010), Determination of permeability from spectral induced polarization in granular media, *Geophys. J. Int.*, *181*(3), 1480–1498.
- Revil, A., and A. Jardani (2013), *The Self-Potential Method, Theory and Applications in Environmental Geosciences*, Cambridge Univ. Press, Cambridge, U. K.
- Revil, A., and H. Mahardika (2013), Coupled hydromechanical and electromagnetic disturbances in unsaturated clayey materials, *Water Resour. Res.*, *49*, 744–766, doi:10.1002/wrcr.20092.
- Revil, A., H. Schwaeger, L. M. Cathles, and P. Manhardt (1999), Streaming potential in porous media. 2: Theory and application to geothermal systems, *J. Geophys. Res.*, *104*(B9), 20,033–20,048.
- Revil, A., V. Naudet, J. Nouzaret, and M. Pessel (2003), Principles of electrography applied to self-potential electrokinetic sources and hydrogeological applications, *Water Resour. Res.*, *39*(5), 1114, doi:10.1029/2001WR000916.
- Revil, A., N. Linde, A. Cerepi, D. Jougnot, S. Matthäi, and S. Finsterle (2007), Electrokinetic coupling in unsaturated porous media, *J. Colloid Interface Sci.*, *313*(1), 315–327, doi:10.1016/j.jcis.2007.03.037.
- Revil, A., M. Karaoulis, T. Johnson, and A. Kemna (2012), Review: Some low-frequency electrical methods for subsurface characterization and monitoring in hydrogeology, *Hydrogeol. J.*, *20*(4), 617–658, doi:10.1007/s10040-011-0819-x.
- Revil, A., M. Skold, S. Hubbard, Y. Wu, D. Watson, and M. Karaoulis (2013), Petrophysical properties of saprolites from the Oak Ridge Integrated Field Research Challenge site, Tennessee, *Geophysics*, *78*(1), D21–D40, doi:10.1190/geo2012-0176.1.
- Rizzo, E., B. Suski, A. Revil, S. Straface, and S. Troisi (2004), Self-potential signals associated with pumping tests experiments, *J. Geophys. Res.*, *109*, B10203, doi:10.1029/2004JB003049.

- Semenov, A. S. (1980), *Elektrorazvedka Metodom Estestvennogo Elektricheskogo Polia*, 2nd ed., 445 pp., Nedra, Leningrad, Russia.
- Sheffer, M. R. (2007), Forward modeling and inversion of streaming potential for the interpretation of hydraulic conditions from self-potential data, PhD thesis, Univ. of Br. Columbia, Canada.
- Sill, W. R. (1983), Self-potential modeling from primary flows, *Geophysics*, *48*, 76–86.
- Stern, O. (1924), Zur Theorie der elektrolytischen Doppelschicht (The theory of the electrolytic double shift), *Z. Elektr. Angew. Phys. Chem.*, *30*, 508–516.
- Straface, S., T.-J. Yeh, J. Zhu, S. Troisi, and C. H. Lee (2007), Sequential aquifer tests at a well field, Montalto Uffugo Scalo, Italy, *Water Resour. Res.*, *43*, W07432, doi:10.1029/2006WR005287.
- Straface, S., E. Rizzo, and F. Chidichimo (2010), Estimation of hydraulic conductivity and water table map in a large-scale laboratory model by means of the self-potential method, *J. Geophys. Res.*, *115*, B06105, doi:10.1029/2009JB007053.
- Straface, S., F. Chidichimo, E. Rizzo, M. Riva, W. Barrash, A. Revil, M. Cardiff, and A. Guadagnini (2011), Joint inversion of steady-state hydrologic and self-potential data for 3D hydraulic conductivity distribution at the Boise Hydrogeophysical Research Site, *J. Hydrol.*, *407*(1–4), 115–128.
- Sun, N.-Z., and W. W.-G. Yeh (1990), Coupled inverse problems in groundwater modeling. 2: Identifiability and experimental design, *Water Resour. Res.*, *26*(10), 2527–2540.
- Suski, B., E. Rizzo, and A. Revil (2004), A sandbox experiment of self-potential signals associated with a pumping-test, *Vadose Zone J.*, *3*, 1193–1199.
- Suski, B., A. Revil, K. Titov, P. Konosavsky, C. Dagès, M. Voltz, and O. Huttel (2006), Monitoring of an infiltration experiment using the self-potential method, *Water Resour. Res.*, *42*, W08418, doi:10.1029/2005WR004840.
- Titov, K., A. Revil, P. Konosavsky, S. Straface, and S. Troisi (2005), Numerical modeling of self-potential signals associated with a pumping test experiment, *Geophys. J. Int.*, *162*, 641–650.
- Troisi, S., C. Fallico, S. Straface, and E. Migliari, (2000), Application of kriging with external drift to estimate hydraulic conductivity from electrical-resistivity data in unconsolidated deposits near Montalto Uffugo, Italy, *Hydrogeol. J.*, *8*(4), 356–367, doi:10.1007/s100400000083.
- Vasco, D. W., A. Datta-Gupta, and J. C. S. Long (1997), Resolution and uncertainty in hydrologic characterization, *Water Resour. Res.*, *33*(3), 379–397.
- Vinogradov, J., and M. D. Jackson (2011), Multiphase streaming potential in sandstones saturated with gas/brine and oil/brine during drainage and imbibition, *Geophys. Res. Lett.*, *38*, L01301, doi:10.1029/2010GL045726.
- von Smoluchowski, M. (1903), Contribution à la théorie de l'endosmose électrique et de quelques phénomènes corrélatifs, *Bull. Int. Acad. Sci. Cracovie*, *8*, 182–200.
- Yeh, T.-C. J., M. Jin, and S. Hanna (1996), An iterative stochastic inverse approach: Conditional effective transmissivity and head fields, *Water Resour. Res.*, *32*(1), 85–92.
- Zhang, J., and T.-C. J. Yeh (1997), An iterative geostatistical inverse method for steady flow in the vadose zone, *Water Resour. Res.*, *33*(1), 63–71.
- Zhu, Z., and M. N. Toksöz (2012), Experimental measurements of streaming potential and seismoelectric conversion in Berea sandstone, *Geophys. Prospect.*, *61*(3), 688–700, doi:10.1111/j.1365-2478.2012.01110.x.